PRIMORDIAL NON-GAUSSIANITY AND THE NRAO VLA SKY SURVEY

JUN-QING XIA[1], MATTEO VIEL[2,3], CARLO BACCIGALUPI[1,2,3], GIANFRANCO DE ZOTTI[1,4], SABINO MATARRESE[5,6] & LICIA VERDE[7]

Draft version June 11, 2010

ABSTRACT

The NRAO VLA Sky Survey (NVSS) is the only dataset that allows an accurate determination of the auto-correlation function (ACF) on angular scales of several degrees for active galactic nuclei at $z \simeq 1$. Surprisingly, the ACF is found to be positive on large scales while, in the framework of the standard hierarchical clustering scenario with Gaussian primordial perturbations it should be negative for a redshift-independent effective halo mass of order of that found for optically selected quasars. We show that a small primordial non-Gaussianity can add sufficient power on very large scales to account for the observed NVSS ACF. The best-fit value of the parameter $f_{\rm NL}$, quantifying the amplitude of primordial non-Gaussianity of local type, is $f_{\rm NL} = 62 \pm 27$ ($1\,\sigma$ error bar) and $25 < f_{\rm NL} < 117$ ($2\,\sigma$ confidence level), corresponding to a detection of non-Gaussianity significant at the $\sim 3\,\sigma$ confidence level. The minimal halo mass of NVSS sources is found to be $M_{\rm min} = 10^{12.47 \pm 0.26} h^{-1} M_{\odot}$ ($1\,\sigma$) strikingly close to that of optically selected quasars. We discuss caveats and possible physical and systematic effects that can impact on the results.

Subject headings: cosmological parameters - cosmology: theory - galaxies: halos - large-scale structure of universe

1. INTRODUCTION

The investigation of primordial non-Gaussianity offers a powerful way of testing the generation mechanism of cosmological perturbations in the early universe. Although the standard single-field, slow-roll, canonical kinetic energy and adiabatic vacuum state inflation generate very small non-Gaussianity, any inflationary model that deviates from this may entail a larger level of it (Bartolo et al. 2004; Komatsu et al. 2009, and references therein).

Deviations from Gaussian initial conditions are commonly taken to be of the so-called local type and parameterized by the dimensionless parameter $f_{\rm NL}$:

$$\Phi = \phi + f_{\rm NL} \left(\phi^2 - \langle \phi^2 \rangle \right) \ , \tag{1}$$

where Φ denotes Bardeen's gauge-invariant potential and ϕ is a Gaussian random field. In this Letter, we use the cosmic microwave background (CMB) convention for the quoted $f_{\rm NL}$ values.

A method (Dalal et al. 2008; Matarrese & Verde 2008) for constraining non-Gaussianity from large scale structure (LSS) surveys exploits the fact that the clustering of extrema (i.e., dark matter halos where galaxies form) on large scales increases (decreases) for pos-

itive (negative) $f_{\rm NL}$. In particular, a non-Gaussianity described by Equation (1) introduces a scale-dependent boost of the halo power spectrum proportional to $1/k^2$ on large scales ($k < 0.03\,h/{\rm Mpc}$), which evolves roughly as $(1 + z)$.

Extragalactic radio sources are uniquely well suited to probe clustering on the largest scales: (1) radio surveys are unaffected by dust extinction which may introduce spurious features reflecting the inhomogeneous extinction due to Galactic dust; (2) due to their strong cosmological evolution, radio sources are very rare locally, so that radio samples are free from the profusion of local objects that dominate optically selected galaxy samples and tend to swamp very large-scale structures at cosmological distances; (3) thanks to the strong cosmological evolution, even shallow radio surveys reach out to substantial redshifts. The NRAO VLA Sky Survey (NVSS; Condon et al. 1998) offers the most extensive sky coverage (82% of the sky to a completeness limit of about 3 mJy at 1.4 GHz) with sufficient statistics to allow an accurate determination of the auto-correlation function (ACF), $w(\theta)$, on scales of up to several degrees (Blake & Wall 2002; Overzier et al. 2003).

When a realistic redshift distribution of the NVSS sources is adopted, the interpretation of the measured $w(\theta)$ in the framework of the standard hierarchical clustering scenario with Gaussian primordial perturbations requires an evolution of the bias factor radically different from that of optically selected QSOs (Negrello et al. 2006; Massardi et al. 2010), in stark contrast with the similar evolution of the luminosity function. In fact, the observed $w(\theta)$ is positive up to large ($\sim 10°$) angular scales, which, for the median source redshift ($z_{\rm m} \simeq 1$), correspond to linear scales where the correlation function should be negative (see also Hernandez-Monteagudo (2009)). Here, we explore whether the (scale-dependent) large-scale non-Gaussian halo bias could reproduce the

[1] Scuola Internazionale Superiore di Studi Avanzati, Via Bonomea 265, I-34136 Trieste, Italy; xia@sissa.it.
[2] INAF-Osservatorio Astronomico di Trieste, Via G.B. Tiepolo 11, I-34131 Trieste, Italy.
[3] INFN/National Institute for Nuclear Physics, Via Valerio 2, I-34127 Trieste, Italy.
[4] INAF-Osservatorio Astronomico di Padova, Vicolo dell'Osservatorio 5, I-35122 Padova, Italy.
[5] Dipartimento di Fisica "G. Galilei", Università di Padova, Via Marzolo 8, I-35131 Padova, Italy.
[6] INFN, Sezione di Padova, Via Marzolo 8, I-35131 Padova, Italy.
[7] ICREA(Institució Catalana de Recerca i Estudis Avançats) and Instituto de Ciencias del Cosmos, Universidad de Barcelona, Marti i Franques 1, 08028, Barcelona, Spain.

observed shape of the NVSS sources ACF, preserving the kinship with optically selected active galactic nuclei (AGNs).

2. NVSS AUTO-CORRELATION FUNCTION

We include in our analysis only NVSS sources brighter than 10 mJy, excluding the strip at $|b| < 5°$, where the catalog may be substantially affected by Galactic emissions. This ensures a uniform sky coverage (Blake & Wall 2002); the effect of possible residual large-scale gradients producing and offset of the ACF is discussed in §4. The NVSS source surface density at this threshold is $16.9 \, \mathrm{deg}^{-2}$. The redshift distribution has recently been determined by Brookes et al. (2008). Their sample, complete to a flux density of 7.2 mJy, comprises 110 sources with $S_{1.4\mathrm{GHz}} \geq 10 \, \mathrm{mJy}$, of which 78 (71%) have spectroscopic redshifts, 23 have redshift estimates via the K–z relation for radio sources, and 9 were not detected in the K band and therefore have only a lower limit in z. Here, we have adopted the description given by de Zotti et al. (2010):

$$dN/dz = 1.29 + 32.37z - 32.89z^2 + 11.13z^3 - 1.25z^4 \ . \quad (2)$$

The NVSS maps are pixelized using the HEALPix software package (Górski et al. 2005) with $N_{\mathrm{side}} = 64$, corresponding to $N_{\mathrm{pix}} = 49,152$ pixels with dimensions $0.92° \times 0.92°$.

The ACF estimator $\hat{w}(\theta)$ reads

$$\hat{w}(\theta) = \frac{1}{N_\theta} \sum_{i,j} \frac{(n_i - f_i \bar{n})(n_j - f_j \bar{n})}{\bar{n}^2} \ , \quad (3)$$

where f_i and n_i are the coverage fraction and the number of radio sources in each pixel, respectively; $\bar{n}$ is the expectation value for the number of objects in the pixel (see Xia et al. 2009). The sum runs over all the pixels with a given angular separation θ. The equal weighting used here is nearly optimal because of the uniform NVSS sky coverage and because on large scales the noise is dominated by sample variance. For each angular bin centered around θ, N_θ is the number of pixel pairs separated by an angle within the bin, weighted by the coverage fractions. We used $N_{\mathrm{b}} = 9$ angular bins in the range $1° \leq \theta \leq 8°$ with a linear binning plus another estimate at $\bar{\theta} = 40'$, since below $40'$ the correlation function is affected by multiple source components and above $8°$ the signal may be affected or even dominated by spurious density gradients (Blake & Wall 2002).

We estimated the covariance matrix of the data points using the jackknife re-sampling method (Scranton et al. 2002). We divide the data into $M = 30$ patches, then create M subsamples by neglecting each patch in turn, and in each subsample we measure the ACF. From the M estimates of the ACF functions, we estimate the diagonal (variance) and off-diagonal (covariance) elements of the covariance matrix for $\hat{w}(\theta)$. In Figure 1, we plot the observed NVSS ACF which is consistent with previous estimates using different approaches (e.g. Blake & Wall 2002). For comparison, we also show the best fit theoretical ACF curve for the Gaussian case ($f_{\mathrm{NL}} = 0$) assuming the redshift-independent minimal halo mass M_{min}. Clearly, the curve does not match the observed ACF data on large scales.
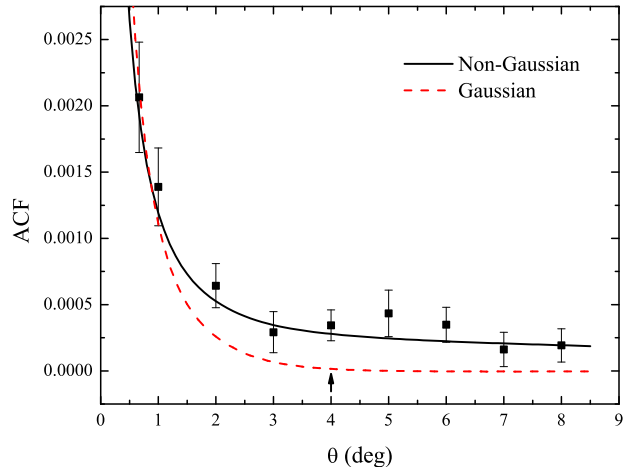

FIG. 1.— Observed ACF of NVSS catalog. Values are jackknife estimated. The black solid line is the best fit model of our non-Gaussian calculations, while the red dashed line refers to the Gaussian case. The vertical arrow marks the angular scale above which the theoretical Gaussian ACF becomes negative. (Here, negative values are not visible, due to their very small amplitudes. See Figure 2 for details.)

Note that the integral over the full survey solid angle covered by the observationally determined ACF vanishes by construction. The estimated values go to zero for $\theta \simeq 30°$, and the non-Gaussian model ACF shown in Figure 1 becomes negative approximately at the same θ. However, no special meaning should be attached to this coincidence since, as noted above, the observational estimate of $w(\theta)$ are unreliable for $\theta \gtrsim 8°$.

3. METHOD

3.1. *Modeling the effects of non-Gaussianity*

The effects of non-Gaussianity on the source clustering properties arise because a non-zero f_{NL} affects the halo mass function and enhances the halo clustering on large scales. The second effect is the dominant one.

In the presence of non-Gaussianity, the mass function $n_{\mathrm{NG}}(M, z, f_{\mathrm{NL}})$ can be written in terms of the Gaussian one $n_{\mathrm{G}}^{\mathrm{sim}}(M, z)$, for which a good fit to the results of simulations is provided by the Sheth-Tormen formula (Sheth & Tormen 1999), multiplied by a non-Gaussian correction factor (Matarrese et al. 2000; LoVerde et al. 2008):

$$R_{\mathrm{NG}}(M, z, f_{\mathrm{NL}}) = 1 + \frac{\sigma_{\mathrm{M}}^2}{6\delta_{\mathrm{ec}}(z)} \cdot$$
$$\cdot \left[S_{3,\mathrm{M}} \left(\frac{\delta_{\mathrm{ec}}^4(z)}{\sigma_{\mathrm{M}}^4} - 2\frac{\delta_{\mathrm{ec}}^2(z)}{\sigma_{\mathrm{M}}^2} - 1 \right) + \frac{dS_{3,\mathrm{M}}}{d\ln\sigma_{\mathrm{M}}} \left(\frac{\delta_{\mathrm{ec}}^2(z)}{\sigma_{\mathrm{M}}^2} - 1 \right) \right], (4)$$

where the normalized skewness of the density field $S_{3,\mathrm{M}} \propto f_{\mathrm{NL}}$, and σ_{M} denotes the rms of the dark matter density field linearly extrapolated to $z = 0$ and smoothed on the scale R corresponding to a Lagrangian radius of a halo of mass M. Here, $\delta_{\mathrm{ec}}(z)$ denotes the critical density for ellipsoidal collapse, which for high peaks is $\delta_{\mathrm{ec}}(z) \sim \delta_{\mathrm{c}}(z)\sqrt{q}$ ($q = 0.75$) and has been calibrated on N-body simulations (Grossi et al. 2009) and
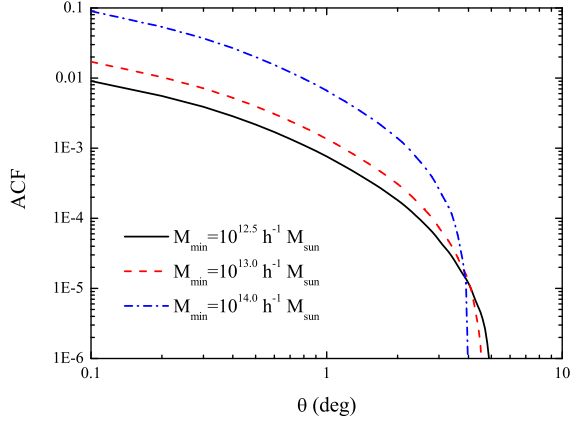
FIG. 2.— Effect of different M_{min} masses on the ACF: the zero-crossing angular scale of the ACF decreases with increasing M_{min} for $f_{NL} = 0$.
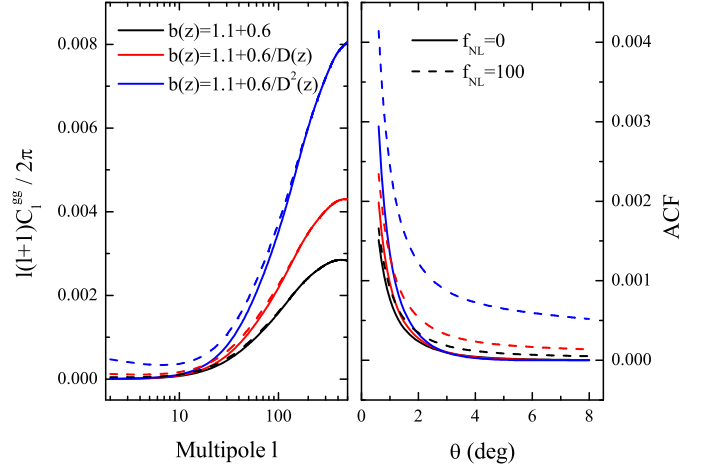

FIG. 3.— Effects of non-Gaussianity on the auto-correlation power spectra (left panel) and on the ACF (right panel) for three different Gaussian bias models.

$\delta_c(z) = \Delta_c(z)D(0)/D(z)$ where $D(z)$ denotes the linear growth factor; $\Delta_c(z) \sim 1.68$ and evolves very weakly with redshift.

More importantly, the large-scale halo bias is also modified by the presence of non-Gaussianity (Dalal et al. 2008; Matarrese & Verde 2008; Grossi et al. 2009):

$$b_{NG}(z) - b_G(z) \simeq 2(b_G(z) - 1)f_{NL}\delta_{ec}(z)\alpha_M(k) , \quad (5)$$

where the factor $\alpha_M(k)$ encloses the scale and halo mass dependence. In practice, we find that, on large scales, $\alpha_M(k) \propto 1/k^2$ and is independent of the halo mass.

We start by assuming that the large-scale, linear halo bias for the Gaussian case is (Sheth & Tormen 1999)

$$b_G = 1 + \frac{1}{D(z_o)}\left[\frac{q\delta_c(z_f)}{\sigma_M^2} - \frac{1}{\delta_c(z_f)}\right]$$
$$+ \frac{2p}{\delta_c(z_f)D(z_o)}\left\{1 + \left[\frac{q\delta_c^2(z_f)}{\sigma_M^2}\right]^p\right\}^{-1} , \quad (6)$$

where z_f is the halo formation redshift, and z_o is the halo observation redshift. As we are interested in massive halos, we expect that $z_f \simeq z_o$. Here, $q = 0.75$ and $p = 0.3$ account for non-spherical collapse and are a fit to numerical simulations (see also Mo & White 1996; Mo, Jing & White 1997; Scoccimarro et al. 2001). We will later relax this assumption.

Finally, the weighted effective halo bias is given by

$$b_{NG}^{eff}(M_{min}, z, k, f_{NL}) = \frac{\int_{M_{min}}^{\infty} b_{NG}n_{NG}dM}{\int_{M_{min}}^{\infty} n_{NG}dM} . \quad (7)$$

Two things should be clear from Equation (5): (1) there is a degeneracy between b_G and f_{NL} (the same amount of non-Gaussian bias can be given by different pairs of b_G, f_{NL} values; strictly speaking, b_G is not a free parameter here, and the degeneracy is between M_{min}, which is a free parameter, and f_{NL}; however b_G is strongly dependent on M_{min}); (2) the $1/k^2$ scale dependence means that large-scales are mostly affected by f_{NL} and small scales are primarily affected by b_G. A positive f_{NL} enhances the amplitude of auto-correlation power

spectra especially at large angular scales ($\ell < 200$, $\theta > 4°$). This is the effect we shall use to constrain f_{NL} and its impact on the ACF is clearly visible in Figure 1. In fact, in the Gaussian case, for the adopted redshift distribution and a redshift-independent M_{min}, the ACF is expected to become negative for $\theta > 4°$. This is also shown in Figure 2 where the ACF is plotted for several values of M_{min}.

In general, the expected degeneracy between f_{NL} and b_G may be lifted in two ways: (1) on small scales the effect of f_{NL} is completely negligible but not that of b_G, (2) the redshift dependences of the two contributions are different. However, the angular correlation function encompasses the signal from different redshifts and different physical scales, complicating the separation of the f_{NL} and b_G signals.

To explore the effect of relaxing the assumption $z_f \simeq z_o$, we have also considered a model for the Gaussian bias given by (Matarrese et al. 1997; Moscardini et al. 1998, and references therein)

$$b_G(z) = b_1 + \frac{b_2}{D^\gamma(z)} \quad (0 \le \gamma \le 2), \quad (8)$$

with b_1 and b_2 being free parameters. Indeed, an "object-conserving" bias model corresponds to $\gamma \approx 1$, while the bias of high-density peaks for objects that have just formed yields $\gamma \approx 2$. In Figure 3, we show the effect of a Gaussian bias model on the auto-correlation power spectra and ACF when varying the power-law index γ; the larger the value of γ the larger is the large-scale non-Gaussian boost.

Lin (2001) and Yoo, Fitzpatrick & Zaldarriaga (2009) discussed the gauge dependence of matter power-spectrum on very large scales ($k < 0.003\,h/Mpc$). We find that this gauge-dependent effect on the matter power spectrum can be mimicked by that of a non-Gaussian halo bias model with $f_{NL} \sim 5$. Here, we calculate the matter power spectrum in the conformal Newtonian gauge.

3.2. *Implementation and data sets*

The theoretical prediction for the ACF depends on: the cosmological parameters, the minimal halo mass $M_{\rm min}$ and $f_{\rm NL}$. For the generalized bias model of Equation (8), we also add the b_1 and b_2 and γ bias parameters.

Rather than fixing the cosmological parameters to the best-fit values derived from Wilkinson Microwave Anisotropy Probe seven year (WMAP7), we will report the results after having marginalized over them with a prior given by a compilation of recent data sets.

We perform a global fitting using the `CosmoMC` package (Lewis & Bridle 2002), a Markov Chain Monte Carlo code, which has been modified to calculate the theoretical ACF. We assume purely adiabatic initial conditions and a flat universe, with no tensor contribution. We vary the following cosmological parameters ($\Omega_b h^2$, $\Omega_c h^2$, τ, Θ_s, n_s, A_s, $f_{\rm NL}$, $M_{\rm min}$), where $\Omega_b h^2$ and $\Omega_c h^2$ are the baryon and cold dark matter densities, τ is the optical depth to reionization, Θ_s is the ratio (multiplied by 100) of the sound horizon at decoupling to the angular diameter distance to the last scattering surface, n_s is the primordial spectral index, and A_s is the primordial amplitude. We do not consider massive neutrinos and dynamical dark energy and for the pivot scale we set $k_{s0} = 0.05\,{\rm Mpc}^{-1}$.

We also use (1) CMB temperature and polarization angular power spectra as measured by WMAP7 (Komatsu et al. 2010), (2) baryonic acoustic oscillations in the galaxy power spectra as measured by the SDSS7 and the Two-degree Field Galaxy Redshift Survey (2dFGRS; Percival et al. 2010) (3) SNIa distance moduli of Union compilation from the Supernova Cosmology Project (Kowalski et al. 2008). We add a prior on the Hubble constant, $H_0 = 74.2 \pm 3.6$ km/s/Mpc (Riess et al. 2009). Finally, we set the minimal halo mass $M_{\rm min} > 10^{12} h^{-1} M_\odot$ consistent with observations showing that radio AGNs are hosted by halos more massive than those hosting optical QSOs (Hickox et al. 2009).

4. RESULTS

We start by considering the case where the Gaussian bias is given by Equation (6). In Figure 4, we show the one-dimensional posterior probability distributions for $M_{\rm min}$ and $f_{\rm NL}$ after marginalizing over the other parameters. The right panel shows the degeneracy between $M_{\rm min}$ and $f_{\rm NL}$. Note that the constraints on $f_{\rm NL}$ only come from the ACF data; external data sets are only used to set the underlying cosmology.

We find that the current ACF implies $f_{\rm NL} > 0$ at the $\sim 3\sigma$ confidence level. The reason for that can be clearly seen in Figure 2 where the Gaussian model with the redshift-independent $M_{\rm min}$ yields an ACF dropping to zero for $\theta \simeq 4°$ and becoming negative on larger scales where the observed ACF is still positive. Non-Gaussianity of the local type adds power on large angular scales yielding a good fit to the observed data points.

The marginalized constraints on the non-Gaussianity parameter $f_{\rm NL}$,

$$f_{\rm NL} = 62 \pm 27 \; (1\,\sigma \;\; {\rm CL}), \qquad (9)$$

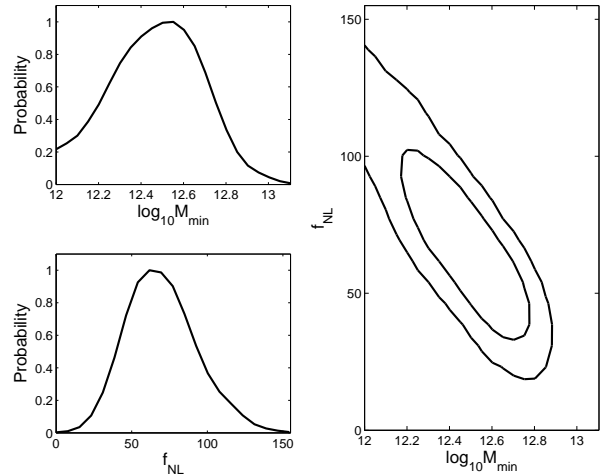$$(6)\,25 < f_{\rm NL} < 117(142) \;\; [95\% \; (99.7\%) \;\; {\rm CL}], \qquad (10)$$

FIG. 4.— Marginalized one-dimensional and two-dimensional distributions (1, 2σ contours) of the minimal halo mass $M_{\rm min}$ and of the non-Gaussian parameter $f_{\rm NL}$.

are compatible with other previous estimates (Yadav & Wandelt 2008; Slosar et al. 2008; Curto et al. 2009; Smidt et al. 2009; Jimenez & Verde 2009; Smith et al. 2009; Rudjord et al. 2009) and in very good agreement with the recent WMAP7 estimate (Komatsu et al. 2010).

The minimal effective halo mass, $M_{\rm min} = 10^{12.47 \pm 0.26} h^{-1} M_\odot$ $(1\,\sigma)$, turns out to be remarkably close to that found for optically selected QSOs: $M_{\rm QSO} = (3.0 \pm 1.6) \times 10^{12} h^{-1} M_\odot$ (Croom et al. 2005).

To explore whether a more general bias model (with γ allowed to conservatively vary even in an un-physical range $\gamma < 1$) than that of Equation (6) may reconcile a Gaussian model with the data, we repeated the analysis using the bias of Equation (8). We keep b_1 and b_2 fixed to 1.1 and 0.6, respectively, and we vary $0 < \gamma < 2$ (the values for b_1 and b_2 have been chosen in order to provide a good fit to the data). In this case, the recovered central value of $f_{\rm NL}$ becomes a little higher and the $1\,\sigma$ error bar increases by about a factor of 2 (a smaller $f_{\rm NL}$ accommodates larger γ and larger bias).

We also perform a cross-check by using the published version of the ACF of Blake & Wall (2002) (in this case zero covariance between data points is assumed, since no covariance matrix has been computed) and find $f_{\rm NL} = 58 \pm 12 \,(1\,\sigma \;\; {\rm CL})$ (we rely on 12 data points in the range $0.5623° \leq \theta \leq 7.70795°$). If we instead set the off-diagonal terms of our ACF estimate to zero, we get $f_{\rm NL} = 70 \pm 15 \,(1\,\sigma \;\; {\rm CL})$. From these results we can conclude that covariance between data points increases the error bar on $f_{\rm NL}$ by almost a factor of 2 and the Blake & Wall (2002) and our ACF measurements are in very good agreement with each other in terms of derived $f_{\rm NL}$ values. Another instructive cross-check is to see to what extent our conclusions are affected by applying an overall subtraction to all the ACF values of 10^{-4}, in order to correct for a possible systematic offset that can contaminate the signal (Blake & Wall 2002). In this case, our constraints are weaker but consistent with the previous analysis and we get $f_{\rm NL} = 42 \pm 30 \,(1\,\sigma \;\; {\rm CL})$.
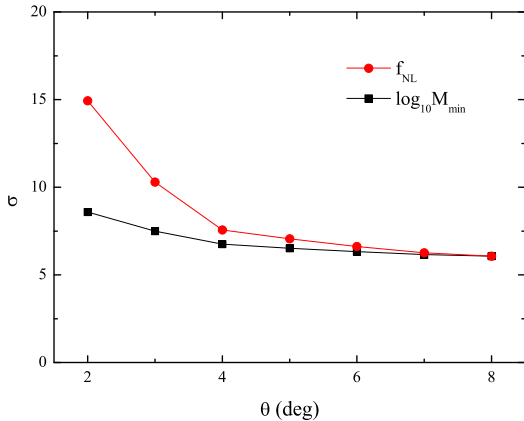
Fig. 5.— Dependence on the maximum separation θ of the error bars on the minimal halo mass $M_{\min}$ and on f_{NL}, calculated with the Fisher matrix method (arbitrary normalization).

We have also checked that the correction proposed by Wands & Slosar (2009) to account for the infrared divergence of the non-Gaussian halo correlation function is negligibly small for our best-fit f_{NL} value.

To allow for the "integral constraint" (measurements probe the survey mean, and not the ensemble mean), we have added to $w(\theta)$ a constant c and have marginalized over c, allowing this quantity to vary in the range $[10^{-8}, 10^{-4}]$ (the upper limit cannot be larger since this is the theoretical variance expected on the scale of the survey scales). We find $f_{\mathrm{NL}} = 58\pm28\,(1\,\sigma)$, showing that, as expected given the large sky fraction covered by the NVSS survey, the best-fit value of f_{NL} is only marginally affected.

We use a Fisher matrix approach to estimate which scales contribute most to the signal for f_{NL} and $\log_{10} M_{\min}$ from the ACF as a function of θ. Depending on where the signal is localized, this may give some insights into what systematic effects are important.

Figure 5 shows the Fisher-predicted error (for the ACF of a survey with NVSS characteristics) as a function of the maximum angle θ (the minimum is always set to $1°$). The error-bar normalization is arbitrary and error bars of f_{NL} and $\log_{10} M_{\min}$ at $\theta = 8°$ are set to be the same. The error on $M_{\min}$ stabilizes at $\theta \sim 3°$, indicating that the bias signal is mainly localized at separations smaller than $3°$. The f_{NL} error decreases rapidly and stabilizes at larger θ, indicating that the non-Gaussian signal is localized in the ACF at $\theta = 2° - 5°$. Since the mean redshift of NVSS sources brighter than 10 mJy is about 1.2, $1°$ corresponds to a comoving size $r \sim 60\,\mathrm{Mpc}$. The maximum non-Gaussianity signal thus comes from comoving scales in the range $120\,\mathrm{Mpc} < r < 300\,\mathrm{Mpc}$, while the constraints on $M_{\min}$ come primarily from scales $r < 180\,\mathrm{Mpc}$.

5. DISCUSSION AND CONCLUSIONS

While previous analyses exploiting the NVSS to constrain primordial non-Gaussianity of local type have focused on the cross-correlation with the WMAP Internal Linear Combination map, we have shown that the angular correlation function alone is a very sensitive non-Gaussianity probe. The key point is that, given the redshift distribution of NVSS, which has been recently observationally determined, and the typical AGN halo mass estimated for optically selected QSOs, the standard ΛCDM cosmology with scale-independent bias would imply, on scales $> 4°$, a negative ACF, but, on the contrary, it is observed to be positive. Careful analyses of the NVSS sample (e.g. Blake & Wall 2002) indicate that systematic offsets that may induce a spurious positive signal should be negligible for the sources with $S_{1.4\mathrm{GHz}} > 10\,\mathrm{mJy}$, selected for the present analysis. If so, the NVSS ACF may point at the presence of a small primordial non-Gaussianity that adds power to the largest scales. After marginalizing over all the other parameters, we find $25 < f_{\mathrm{NL}} < 117$ at the 95% confidence level, compatible with bounds derived by other studies. The minimum halo mass turns out to be $M_{\min} = 10^{12.47\pm0.26}\,h^{-1}\,M_\odot\,(1\,\sigma)$, remarkably close to the value found by Croom et al. (2005) for optically selected QSOs.

We have addressed the significance and the robustness of our findings by considering different bias models and by investigating the impact of gauge effects on large scales. Error bars were estimated by a jackknife re-sampling procedure, widely used in the literature (Scranton et al. 2003; Xia et al. 2009). It is known to be robust and accurate for the diagonal elements of the covariance matrix but not as widely tested and calibrated for the off-diagonal ones, which cannot be neglected because neighboring ACF data points are highly correlated. From Scranton et al. (2003), we infer that jackknife can underestimate parameter errors by up to 30%. If the error bars were to be increased by this (maximal) amount, f_{NL} would become compatible with zero at the $\sim 2\,\sigma$ confidence level. We conclude that our work should be seen as a "proof of principle", indicating that future surveys probing scales ~ 100 Mpc at substantial redshifts can put stringent constraints on primordial non-Gaussianity (e.g. Carbone et al. 2008; Viel et al. 2009).

REFERENCES

Bartolo, N., Komatsu, E., Matarrese, S., & Riotto, A., 2004, Phys. Rep., 402, 103
Blake, C., & Wall, J. 2002, MNRAS, 337, 993

Brookes, M. H., Best, P. N., Peacock, J. A., Rötgering, H. J. A., & Dunlop, J. S. 2008, Mon. Not. Roy. Astron. Soc., 385, 1297
Carbone, C., Verde, L., & Matarrese, S. 2008, Astrophys. J., 684, L1

Condon, J. J., Cotton, W. D., Greisen, E. W., Yin, Q. F., Perley, R. A., Taylor, G. B., & Broderick, J. J. 1998, Astron. J., 115, 1693

Croom, S. M., et al. 2005, Mon. Not. Roy. Astron. Soc., 356, 415

Curto, A., Martinez-Gonzalez, E., & Barreiro, R. B. 2009, Astrophys. J., 706, 399

Dalal, N., Doré, O., Huterer, D., & Shirokov, A. 2008, Phys. Rev. D, 77, 123514

de Zotti, G., Massardi, M., Negrello, M., & Wall, J. 2010, Astron. Astrophys. Rev., 18, 1

Górski, K. M., et al. 2005, Astrophys. J., 622, 759

Grossi, M., et al. 2009, Mon. Not. Roy. Astron. Soc., 398, 321

Hernandez-Monteagudo, C., 2009, arXiv:0909.4294

Hickox, R. C., et al. 2009, Astrophys. J., 696, 891

Komatsu, E., et al. 2009, AGB Stars and Related Phenomena Astro2010: The Astronomy and Astrophysics Decadal Survey, 2010, 158, arXiv:0902.4759

Komatsu, E., et al. 2010, arXiv:1001.4538

Kowalski, M., et al. 2008, Astrophys. J., 686, 749

Jimenez, R., & Verde, L. 2009, Phys. Rev. D, 80, 127302

Lewis, A. & Bridle, S. 2002, Phys. Rev. D, 66, 103511, http://cosmologist.info/cosmomc/

Lin, W. B. 2001, Chin. Phys. Lett., 18, 1539

LoVerde, M., Miller, A., Shandera, S., & Verde, L. 2008, JCAP, 0804, 014

Massardi, M, Bonaldi, A, Negrello, M., Ricciardi, S., Raccanelli, A. & De Zotti, G., 2010, Mon. Not. Roy. Astron. Soc., 404, 532

Matarrese, S., Coles, P., Lucchin, F. & Moscardini, L. 1997 Mon. Not. Roy. Astron. Soc. 286, 115

Matarrese, S., Verde, L., Jimenez, R., 2000, Astrophys. J., 541, 10

Matarrese, S., & Verde, L. 2008, Astrophys. J., 677, L77

Mo, H. J., Jing, Y. P., & White, S. D. M. 1997, Mon. Not. Roy. Astron. Soc., 284, 189

Mo, H. J. & White, S. D. M. 1996, Mon. Not. Roy. Astron. Soc., 282, 347

Moscardini, L., Coles, P., Lucchin F. & Matarrese, S. 1998, Mon. Not. Roy. Astron. Soc., 299, 95

Negrello, M., Magliocchetti, M., & De Zotti, G. 2006, Mon. Not. Roy. Astron. Soc., 368, 935

Overzier, R. A., Röttgering, H. J. A., Rengelink, R. B. & Wilman, R. J. 2003, A&A, 405, 53

Percival, W. J., et al. 2010, Mon. Not. Roy. Astron. Soc., 401, 2148

Riess, A. G., et al. 2009, Astrophys. J., 699, 539

Rudjord, O., Hansen, F. K., Lan, X., Liguori, M., Marinucci, D. & Matarrese, S., 2009, Astrophys. J. , 701, 369

Scoccimarro, R., Sheth, R., Hui, L., & Jain, B. 2001, Astrophys. J., 546, 20

Scranton, R., et al. 2002, Astrophys. J., 579, 48

Scranton, R., et al. 2003, arXiv:astro-ph/0307335

Sheth, R. K. & Tormen, G. 1999, Mon. Not. Roy. Astron. Soc., 308, 119

Slosar, A., Hirata, C., Seljak, U., Ho, S., & Padmanabhan, N. 2008, JCAP, 8, 31

Smidt, J., Amblard, A., Serra, P., & Cooray, A. 2009, Phys. Rev. D, 80, 123005

Smith, K. M., Senatore, L., & Zaldarriaga, M. 2009, JCAP, 0909, 006

Viel, M., Branchini, E., Dolag, K., Grossi, M., Matarrese, S. & Moscardini, L. 2009, Mon. Not. Roy. Astron. Soc., 393, 374

Wands, D. and Slosar, A., 2009, Phys. Rev.D, 79, 123507

Xia, J. Q., Viel, M., Baccigalupi, C., & Matarrese, S. 2009, JCAP 0909, 003

Yadav, A. P. S. & Wandelt, B. D. 2008, Phys. Rev. Lett., 100, 181301

Yoo, Y., Fitzpatrick, A. L., & Zaldarriaga, M. 2009, Phys. Rev. D, 80, 083514